Analysis of gas transport phenomena in a polymer electrolyte fuel cell by electrochemical pressure impedance spectroscopy

Anantrao Vijay Shirsath, Caroline Bonnet, Stéphane Raël, François Lapicque

▶ **To cite this version:**

Anantrao Vijay Shirsath, Caroline Bonnet, Stéphane Raël, François Lapicque. Analysis of gas transport phenomena in a polymer electrolyte fuel cell by electrochemical pressure impedance spectroscopy. Journal of Power Sources, 2022, 531, pp.231341. 10.1016/j.jpowsour.2022.231341 . hal-03827527

HAL Id: hal-03827527
https://hal.science/hal-03827527

Submitted on 24 Oct 2022

HAL is a multi-disciplinary open access archive for the deposit and dissemination of scientific research documents, whether they are published or not. The documents may come from teaching and research institutions in France or abroad, or from public or private research centers.

L'archive ouverte pluridisciplinaire **HAL**, est destinée au dépôt et à la diffusion de documents scientifiques de niveau recherche, publiés ou non, émanant des établissements d'enseignement et de recherche français ou étrangers, des laboratoires publics ou privés.

Analysis of gas transport phenomena in a polymer electrolyte fuel cell by electrochemical pressure impedance spectroscopy

Anantrao Vijay Shirsath, Caroline Bonnet, Stéphane Raël[1], François Lapicque

Université de Lorraine, CNRS, LRGP, F-54000 Nancy, France

[1] Université de Lorraine, GREEN, F-54000 Nancy, France

Abstract:

Electrochemical pressure impedance spectroscopy (EPIS) was introduced in view to differentiating transport/transfer phenomena of gas and liquid occurring in electrochemical cells. This work aimed at measuring EPIS impedance in a 100 cm^2 membrane fuel cell upon predominant control from gas transport, in conditions where the presence of liquid water is little significant. Operating the fuel cell with pure oxygen allowed observation of gas convection: EPIS impedance modulus was below 1 µV Pa^{-1} in the frequency range 1 mHz – 1 Hz, whereas the phase shift decrease did not exceed 30° near 200 mHz with an MPL-free gas diffusion layer (GDL). Conversely, occurrence of diffusion phenomena with oxygen diluted into nitrogen or helium is revealed by the strong increase in the EPIS modulus up to 12-30 µV.Pa^{-1} near 500 mHz depending on the nature of the diluting gas, the GDL, and the excess in fed oxygen. Corresponding phase shift decreased regularly from nearly 0° at 1 mHz to approx. -200° at 1 Hz. The presence of liquid water and its poor management by the MPL-free GDL aggravates gas transport situation in the porous layers, in particular with more negative phase shifts and higher modulus at high frequency.

Keywords: Electrochemical pressure impedance spectroscopy; Proton exchange membrane fuel cell; transport phenomena; gas diffusion; gas convection.

*Corresponding author: francois.lapicque@univ-lorraine.fr

1- Introduction

Asides the catalytic properties of the cathode and the high conductivity of the polymeric membrane, mass transport phenomena in polymer electrolyte membrane fuel cells (PEMFCs) have a strong influence on fuel cell efficiency and energy production rate. Transport phenomena of gases in a FC are principally gas convection and oxygen diffusion in the channels of the bipolar plate or through the catalytic and gas diffusion layers of the fuel cell. Transport of liquid water occurs through the membrane and in the other FC components, depending on its significance and the hydrophobicity level of the considered components. Should the transport rates of gas or liquid be insufficient, the fuel cell performance is controlled by mass transport/transfer phenomena. This very common situation is usually evidenced by the levelling-off of the current density upon increasing overpotential in voltammetric curves or by the appearance of an additional loop at low frequency in Nyquist plot of electrochemical impedance spectra (EIS) [1-4]. The complex impedance calculated by equivalent electric circuit models, involves a resistance and a time constant indicating on the frequency range for this loop. Because of the possible contribution of Knudsen diffusion, diffusion coefficients of gases in the catalytic layer (CL), the microporous layer (MPL) and the macroporous substrate (MPS) are to differ from each other [5]. Time constants for gas diffusion often defined as the square of the layer thickness divided by the diffusion coefficient, are also to be very different. For values of the time constants lower than 100 ms as often in CLs, charge and mass transfer in the vicinity of the catalytic site can appear as a single loop in Nyquist plot, making separate interpretation delicate. Besides, modelling the mass transfer in a GDL comprising an MPL deposited on the MPS, can reveal as inefficient because of the different pore size distributions and permeability exhibited by the two layers [6]. An additional difficulty in modelling is caused by the appreciable penetration of the MPL into the MPS anisotropic structure, a phenomenon rendered more acute for aged GDLs, as exemplified by Figure 1. For the case of liquids for which diffusion coefficients are orders of magnitude below those of gases, time constants are to be far larger than those for gases. Flooding phenomena could thus be evidenced by an inductive loop for frequencies far below 1 Hz [7,8] or by a further larger mass transfer loop [9]. Roy and Orazem [10] could more accurately evidence flooding phenomena by further treatment of the EIS spectra using a stochastic approach.

In most cases, EIS spectra of a fuel cell under operation often exhibit two partly overlapping loops attributed to charge and mass transfers. Two main problems can be encountered in the spectra recorded. First, EIS data for frequency below 10-100 mHz are often scattered because of the insufficient accuracy in the impedance calculation from the current and cell voltage fluctuations, then making investigations of mHz frequencies nearly impossible. Secondly, the single loop covering all mass transfer phenomena is characterized by a single time constant, usually in the range 100 ms – 1 s as reported for instance in [5], rendering difficult the separate analysis of transfer phenomena.

As shown in previous works, development of electrochemical techniques involving one non-electrical variable is to allow complementary information on species transport or transfer phenomena. For this purpose, other physical variables have successfully been used e.g. pulsation of velocity in electrohydrodynamic impedance [11] or the sine weight fluctuations monitored by a quartz balance upon potential modulation [12], or the back-pressure of an electrochemical cell as the oscillating excitation variable [13,14]. This last technique, called electrochemical pressure impedance spectroscopy (EPIS), was shown to be promising in complement to regular EIS [15,16] for better understanding of transport phenomena in electrochemical cells involving the presence of gases. A fuel cell test bench was previously developed to implement EPIS technique by superimposing outlet pressure fluctuations in the range 1 mHz – 1 Hz to the steady outlet pressure and monitoring the induced fluctuations of the voltage at a fixed current [17]. The particular impedance $Z_{U\text{-}P}$, defined as the ratio of the voltage complex fluctuations over those of the outlet pressure, was observed depending on the operating conditions: current density, hydration conditions in the fuel cell and oxygen content in the nitrogen-oxygen gas mixture fed. Frequency variations of the $Z_{U\text{-}P}$ modulus and the phase shift φ recorded for suitable operated conditions allowed to evidence separately the occurrence of water transport for frequencies below 30-50 mHz, and transport phenomena involving gas over 30 mHz [17,18].

In view to complementing the preliminary results previously reported, the present work aimed at focusing on gas transport and transfer by diffusion and convection. For this purpose, the significance of liquid water in the porous regions of the fuel cell and the channels of the bipolar plates was kept as low as possible, to avoid occurrence of two-phase flow in these regions. The effect of three operational parameters has been investigated in this work. First, the nature of the

GDL was changed, depending on whether a microporous layer (MPL) is attached on the macroporous substrate or not – which is also to affect gas convection in the GDL. Secondly, the air oxygen stoichiometry was varied to change gas convection rates in the channels and in the gas diffusion layers (GDL). Finally, the nature of the oxygen diluting gas was also changed, by replacing nitrogen in air or other (N_2-O_2) gas mixtures by helium. Because of its diffusivity four times lower than that of nitrogen, diffusion phenomena are to be less rate controlling in fuel cells with (He-O_2) mixtures, as investigated formerly by voltammetry [19–21] or EIS [22].

2- Experimental section

2.1. Fuel cell and test bench

Experimental work has been carried out in a test bench previously described [5, 23]. The fuel cell was a single 100 cm^2 cell (UbzM, Ulm, Germany). The flow pattern of the two bipolar plates consisted of 23 parallel channels (0.5 x 0.4 mm^2) covering the plate surface in a multiple serpentine (3 passes) profile without gas collecting manifolds. The overall length of one channel was near 35 cm. The membrane electrode assembly (MEA) consisted in a 20 µm thick Gore membrane and two gas diffusion electrodes (GDE) with a Pt loading at 0.4 mg cm^{-2} at the cathode and 0.1 mg cm^{-2} at the anode. GDLs (Sigracet, Germany) were either of 34 BA grade, i.e. without MPL, or of 29 BC (more recent) grade comprising an MPL. Characteristic parameters and properties of the two GDLs are given in Table 1. The GDL inserted in the anodic chamber was of 29 BC grade in all cases. The cell was installed into the flow rig provided with gas humidifiers for the two gas streams fed, and at the cell outlet condensers at 5°C for the recovery of water present in the exhaust gases and to protect the release valves [17]. Off gases were driven to the fume hood.

2.2. Fuel cell operation

The cell was operated at 55°C and 150 mbar above the atmospheric level at both anode and cathode outlets. To avoid too significant formation and accumulation of liquid water in the fuel cell, the current density was restricted to 0.2 A cm^{-2}. Dry hydrogen was fed with a stoichiometric factor λ_{H2} fixed at 1.2. Air was humidified at a relative humidity (RH) of 20% only, with a stoichiometric factor λ_{O2} varying from 1.5 to 4, λ_{O2} = 2.5 being the "nominal" stoichiometric

factor. In some experiments, air was replaced by pure oxygen or by (N_2-O_2) or (He-O_2) mixtures of various O_2 contents. For O_2 contents different from the regular content in air (21%), the oxygen stoichiometry was changed, so that the volume flow rate of gas fed to the cathode be the same as that with regular air. Thus, the velocity of the gas in the channels and its residence time in the cathodic chamber were kept constant. Hence, $\lambda_{O2} = 11.9$ with pure oxygen is to allow the same flow conditions in the cell as $\lambda_{O2} = 2.5$ with air. Besides, from the amounts of water collected from the condensers and the inlet relative humidity, water mass balances allowed the fraction of water actually in liquid form at the outlet of the cathode chamber to be determined together with the amount of water transferred from the cathode side to the anode side.

2.3. Operation with outlet pressure fluctuations

Outlet pressure of the anode compartment was kept to 150 mbar above the ambient level, whereas at the cathode side, pressure fluctuations were superimposed to the steady relative 150 mbar by the dSPACE control system implemented on the bench PC. In addition to the above fluctuations of the outlet pressure, this control system was used to control the cell operation at fixed current and to monitor operating variables, in particular pressure and voltage fluctuations. Data acquisition was filtered to avoid electrical noise from harmonics following a procedure developed beforehand: two filters at 1 and 20 mHz were used for all measurements, and for frequency below 100 mHz, the signals were further submitted to a dynamic filter. Data were recorded for 4 to 200 periods depending on the frequency for the sake of reduced electrical noise: in-house MATLAB-Simulink programs were used for this purpose. As previously detailed [17], care was taken in the selection of the amplitude of outlet pressure sine fluctuations so that the voltage response followed sine fluctuations at the same frequency, with minimal signal distortion while allowing voltage amplitude larger than 1 mV, i.e. at least one decade larger than the signal noise. The excitation amplitude to be used was found to strongly depend on the frequency, being far larger for low frequencies (at a few mHz) than over 100 mHz. Amplitude and phase shift of the first harmonic signal – corresponding to EPIS impedance – were obtained by fitting the filtered data to the theoretical harmonics. Uncertainty in $Z_{U\text{-}P}$ modulus was estimated by simulation to be in the order of 5% at low frequency and up to 8-10% for frequencies larger than 100 mHz. With regards to its phase shift, the uncertainty was estimated to be in the order of 2°. Most spectra were replicated at least once.

3- Results and discussion

The EPIS response of the membrane electrode assembly with its GDLs was shown to be dependent on its state of health, since fuel cells naturally undergo degradation of their components, and recording a whole spectrum required on average 6 hours. Therefore, for investigation of the effect of one operating parameter or condition, all tests have been carried out in a time period, for which the fuel cell had a comparable state of health. The state of health related to the FC performance, was checked at regular intervals by electrochemical voltage measurements at fixed current density and EIS at various current densities [24]. However, the EPIS response for the "reference case" with air at λ=2.5 could vary with the operating conditions investigated, because of different states of health of the cell. In case of insufficient performance of the fuel cell, the MEA was replaced, so the reference case had to be further recorded after maturation of the MEA.

3.1. Effect of the microporous layer in the GDL

The presence of MPL at the cathode deposited on the microporous substrate is to improve water management in the fuel cell, acting as a barrier to water thus avoiding liquid penetration due to the higher capillary pressure in the MPL than in the MPS. Presence of an MPL is also to change the thermal resistance of the MEA, modifying the local temperature at the GDL/CL boundary thus the amount of liquid water in the MEA. The fuel cell can thus tolerate higher gas hydration and higher water production when subjected to large currents. Another expected effect of this operational parameter is the nature of transport phenomena as explained as follows. The two GDLs exhibit very different permeability values; through plane transport in 34 BA being nearly 2 orders larger than that in 29 BC [25] due to the presence of the MPL. Therefore, it may be considered that whereas convection phenomena are of appreciable importance in the 34 BA GDL far from the electrode surface, diffusion becomes predominant in the 34 BA-electrode interface. On the contrary, gas transfer in the 29 BC MPL is to occur nearly exclusively by diffusion.

Tests with pure oxygen

First, tests were carried out with pure oxygen to avoid diffusion of oxygen in a different gas. Although diffusion phenomena induced by local change in pressure can also occur with pure oxygen, working without O_2 diluting gases in the cathode chamber should allow clearer observation of convection phenomena by pressure-induced impedance spectroscopy. To limit the significance of liquid water in the cell, the oxygen stoichiometric factor was set at 11.9. As a matter of fact, it was estimated from mass balances that approx. 22% of the water leaving the cathode chamber was in the liquid form whatever the GDL tested. As shown in Figure 2a, the modulus of the voltage-over-pressure impedance with 34 BA was approx. 20% larger below 80 mHz than with 29 BC whereas the comparison was inverted for larger frequencies. At low frequency, the observed comparison can be the fact of more troublesome transport of liquid water in the fuel cell, in spite its moderate significance. The indirect negative effect of liquid water on gas transfer rates was also observed using EIS by Owejan et al. [26]. For larger frequencies, the easier convection phenomena with MPL-free 34 BA are to result in lower impedance moduli, as observed by experiments (Figure 2a). Nevertheless, the differences in impedance are moderate and so is its modulus, below 0.6 $\mu V\ Pa^{-1}$ with either of the GDLs tested. With regards to the phase shift, the absence of diffusion phenomena of oxygen in nitrogen causes moderate variations of the phase shift as observed previously [17], being in the range +5 / -15° with 29 BC GDL (Figure 2b). By using 34 BA GDL, the phase shift peaking at -30° at 100 mHz, might be related to uneven gas distribution in the coarser structure of this GDL. From this series of experiments, convection phenomena can be observed by EPIS moduli at frequencies larger than 80 mHz. Characteristic time for gas convection, τ_{conv}, in the channel can be defined as its residence time: from the dimensions of the flow pattern given in Section 2.1, τ_{conv} was shown to be near 0.12 s at 0.2 A cm^{-2}. In the GDL, the characteristic time can be defined as the ratio of the thickness over the velocity of the reacting gas passing from the channels through the GDL, in the order of 1 mm/s at 0.2 A/cm^2 [25], thus found in the order of 0.2 s. Both time estimates are consistent with the above frequency domain for gas convection. However, EPIS signals corresponding to occurrence of convection, seem to be of a moderate significance, with restricted changes in the impedance modulus and little effect on its phase shift.

Tests with air

As observed previously with air, or low O_2 containing gas mixtures [5,6], Z_{U-P} modulus remains lower than 1 µV Pa^{-1} at frequencies below 10 mHz (Figure 3). Beyond this frequency, a strong increase in Z_{U-P} modulus is observed with the presence of a flat maximum near 400 mHz. In both cases, larger modulus was measured with the MPL-free GDL than with 29 BC grade. At low frequency, this fact of a moderate significance could be caused by the better water management allowed by the presence of the MPL which facilitates transport of liquid water in the porous layers. The difference in behavior exhibited by the two GDL becomes more visible beyond 10 mHz: whereas the maximum impedance modulus with 29 BC attained 6 µV Pa^{-1}, the modulus with MPL-free 34 BA was measured at 14 µV Pa^{-1}. Moreover, this observation is consistent with the lower mass transfer resistance of MEA provided with an MPL as reported in [6]. The situation could be aggravated by the presence of liquid water at the cathode - although with a fraction only near 22% at the cell outlet- with the two GDLs, but whose management is far worse with the MPL-free 34 BA. It is possible that with 34 BA GDL the macroporous layer in the vicinity of the electrode be partly obstructed by water droplets, forcing the gas to be transported through narrower paths, which is to result in larger Z_{U-P} modulus. The phase shift measured with both GDLs was found to decrease nearly linearly with the log of the frequency (Figure 3), attaining -210° at 1 Hz, as observed previously for other EPIS measurements with air fed to the cathode [17].

EIS spectra recorded at 0.2 A cm^{-2} were affected by the nature of the GDL (Figure 4). The poorer water management with 34 BA GDL is shown at high frequency, with larger ohmic and charge transfer resistances, likely caused by the uneven distribution of liquid water. Moreover, a larger low frequency-loop was also obtained with the MPL-free GDL. Interpretation of the spectra using an equivalent circuit model with an overall Warburg element covering finite diffusion in the GDL and the catalyst layer (CL), led to a diffusion resistance 65% larger with the 34 BA GDL than with the other GDL.

3.2. Effect of air oxygen stoichiometry

The flow rates of air fed to the cell was varied so that λ_{O2} could vary from 1.5 to 4. The cathode compartment was provided with a 29 BC GDL. Mass balances in the fuel cell for oxygen and water showed that the O_2 fraction in the cathode outlet gas varies from 7.0% for λ_{O2} = 1.5 to

14.6% for λ_{O2} = 4. In the meanwhile, liquid water is not present for the highest λ_{O2} value but was shown to represent 45% of the overall water leaving the cathodic chamber for λ_{O2} = 1.5. Therefore, increasing the air stoichiometry does not only modify the gas velocity in the channels but also through-plane or in-plane flow in the GDL. It is also to affect oxygen concentration profiles – thus the rate of diffusion phenomena.

The EPIS spectra in Bode plots are shown in Figure 5. As observed above with air, Z_{U-P} modulus remains in the order of 1 µV Pa^{-1} at 4 mHz or below, then increases steadily from 10 mHz to attain a very flat maximum near 500 mHz (Figure 5a). However, the increase in modulus with increasing frequency depends strongly on the air stoichiometric factor: the maximum of the impedance modulus being only at 2.5 µV Pa^{-1} for the largest O_2 excess, passed to nearly 10 µV Pa^{-1} for λ_{O2} = 2.5, and to 27 µV Pa^{-1} for λ_{O2} = 1.5. In the meanwhile, depending on $\lambda_{O2,}$ the phase shift followed nearly parallel decreasing variations with the frequency (Figure 5b) down to values in the order of -200°. Reducing the oxygen excess in the fuel cell is accompanied by a shift of the decreasing variation to more negative phase shifts. Conversely, with the highest λ_{O2} value, the phase remains nearly nil up at 4 mHz, then departs to negative values from this frequency.

Both very high impedance moduli and strongly negative phase shifts were attributed to diffusion phenomena from EPIS tests carried out with (N_2-O_2) mixtures with different O_2 contents and with 29 BC GDL [17]. Such explanation also holds for this series of experiments since more rate-controlling diffusion phenomena are to occur when oxygen is highly depleted from the gas phase in the fuel cell as for low λ_{O2}. However, and in spite of its moderate significance in this GDL, this might also be the fact of more troublesome convection for low stoichiometric factors. An additional factor to be accounted for here, is the appreciable fraction of liquid water in the fuel cell for the lowest stoichiometric factor. In such conditions, the porous layers and the bipolar plate channels might be partly obstructed by water droplets or puddles, forcing the gas to be transported through narrower paths, then making both convection and diffusion phenomena more problematic. Combination of the two gas transport phenomena to their hindrance by liquid water would cause such high impedance values.

3.3. Effect of the nature of the oxygen diluting gas

A 29 BC GDL was mounted in the cathodic compartment. Oxygen content was either at 21% or 50% in nitrogen or in helium. For reasons expressed above, the stoichiometric factor for oxygen was not at the same levels to maintain the same flow rate of gas for the two dilution factors. For both oxygen contents, the divergence between the variations plotted for two diluting gases is clearly visible from 100 mHz (Figure 6). Besides, as observed previously with N_2-O_2 mixtures [5], $Z_{U\text{-}P}$ strongly decreases with the increase in the oxygen molar fraction in helium for frequencies larger than 100 mHz (Figure 6).

For low frequencies, the profiles of the EPIS modulus are little affected by the nature of the diluting gas. However, for $y_{O2} = 0.50$, measured moduli below 100 mHz were somewhat larger with helium than with nitrogen (Figure 6b), being near 0.6 and 0.4 µV Pa^{-1} at 1 mHz respectively. In spite of the small amount of liquid water formed (in the order of 22% at the cell outlet), the above observation could be explained by former works on water droplet detachment from the GDL surface depending on whether that ambient gas was nitrogen or helium [27]. Because of helium's restricted density, the forces exerted on the droplet resulting to its deformation and its more rapid detachment, are less significant than those with comparable O_2-N_2 flow in the channel. Thus, nitrogen-based mixtures would appear more efficient than helium-based mixtures in the evacuation of liquid droplets emerging from the GDL which may result in lower $Z_{U\text{-}P}$ moduli at low frequency.

Higher $Z_{U\text{-}P}$ moduli were observed for frequencies larger than 100 mHz with nitrogen, with a difference in the order of 20%. This difference could be related to the compared oxygen diffusion coefficient in the two diluting gases, as well as the GDL permeability in these gases. The effective diffusivity of oxygen in He or N_2 at the fuel cell temperature and pressure was evaluated in the MPS and MPS of the GDL, as well as in the catalytic layer (CL) (Appendix). The values obtained reported in Table 2 illustrate the advantages allowed by helium, with O_2 equivalent diffusivity approx. 4 times larger than in nitrogen. Besides, the permeability values of the GDL in through plane transport, K_v, for the two pure diluting gases were taken from [25]: permeability of the GDL for the gas mixtures was estimated as the weighted average of K_v values for oxygen (assumed to be equal to that of nitrogen) and that with the diluting gas. Permeability K_v of 29 BC gas diffusion layer was thus constant at 1.97 10^{-13} m^2 in N_2-O_2 mixtures whatever the O_2 content, and was found at 4.43 and 3.53 10^{-13} m^2 in He-O_2 mixtures with 21% and 50% O_2 respectively.

The above positive action of helium in comparison to nitrogen for frequencies larger than 100 mHz, can be related to former observations made with electrochemical techniques. The experimental variations of the voltage with the current density of a small PEM fuel cell [22] for various partial pressures of oxygen, were interpreted considering a Koutecky-derived law, involving a kinetically controlled current density together with a limiting current density. Assuming the same Tafel law for the kinetic term for the two diluting gases, fitting of the data yielded limiting current density at 3.62 and 5.75 A cm^{-2} bar^{-1} O_2 with nitrogen and helium respectively. Besides, EIS spectra of the cell fed with fully humidified air or heliox (21% O_2 in He) were interpreted using the above equivalent circuit model, with a single loop for mass transfer phenomena in the various layers. The diffusion resistance involved in the Warburg expression for O_2 transfer was found near 77 mΩ cm^2 with helium and 180 mΩ cm^2 with nitrogen. EIS spectra recorded with our fuel cell system reported in Figure 7 also show a larger loop at frequencies below 20 Hz for air than for heliox. Interpretation of these spectra yielded diffusion resistances respectively at 150 and 269 mΩ cm^2, in qualitative agreement with the spectra recorded by Cruz-Manzo and Greenwood [22]. Moreover, characteristic time τ was found from Figure 7 to be near 0.148 s with helium and 0.169 s with nitrogen.

Aside characteristic convection times estimated in Section 3.1 at 0.04 and 0.25 s in the channel and through the GDL, the estimates for the diffusion coefficient taking into account Knudsen diffusion and reported in Table 2, led to characteristic time for diffusion, τ_{diff}, using relation (A5) equal to 1.8, 17 and 211 ms respectively in the CL, MPL and MPS for nitrogen. With helium as the diluting gas, these estimates are approx. three times lower (Table 2). However, these estimates for O_2 diffusivity in the order of 10^{-6} m^2 s^{-1}, are likely overestimated because of the complex morphology of these three layers and of their interface with the possible presence of liquid water. From EIS measurements, Kulikovski et al. [28] estimated an overall diffusion coefficient in the order of 10^{-8} ms^{-1} in the CL, far below the above estimations. The overall characteristic time τ calculated from Figure 7 is likely the resultant of the combined effects of gas transport together with diffusion of oxygen within the ionomeric layer near the catalyst site, in accordance with the equivalent diffusion coefficient reported in [28]. The two diluting gases tested exhibit nevertheless comparable behaviors, even though the mass transfer resistance in EIS is two times larger with air than with Heliox. This stronger difference could also be linked

to the difference in GDL permeability to the diluting gases, near 25 % for the case of air and heliox in addition to the difference in diffusion coefficient.

In spite of the above interpretation based on different diffusion coefficient and GDL permeability values with the two gases, it has to be recognized that convection and diffusion phenomena could not be clearly distinguished from each other from this series of experiments.

4- Conclusion

Gas transport and transfer phenomena in a PEM fuel cell have been investigated using electrochemical pressure impedance spectroscopy for low hydration conditions. Customized experiments have been designed and carried out to distinguish EPIS signals from the occurrence of convection and diffusion. Convection could be separately tackled by operating the cell with pure oxygen: EPIS signals were shown to be of a little intensity in the frequency domain 10 mHz – 1 Hz, both in their intensity (modulus) and phase shift. Occurrence of diffusion with air feed is far more visible by EPIS for frequencies over 10 mHz, as shown by the steady decrease of the gas shift from nearly 0° at 1 mHz, to approx. -200° at 1 Hz and by a broad modulus peak near 500 mHz. In addition, the level of the modulus maximum is increased by higher rate-controlling diffusion, as with low O_2 contents in the gas fed to the cathode, or with lower stoichiometric factor of air oxygen. Replacing nitrogen by helium of a higher molecular diffusivity facilitates oxygen transfer toward the catalytic sites as revealed by the lower EPIS impedance modulus at high frequencies, in agreement with EIS spectra. Finally, the signals generated by the occurrence of the two gas transfer phenomena (convection and diffusion) could be amplified in situation where the (restricted) amount of liquid water in the fuel cell hinders gas transport in the porous layers, as observed when using GDL with poor water management capacities as with MPL-free gas diffusion layers.

Acknowledgment:

The authors would like to thank the ANR-EPISTEL (ANR-17-CE05-0031) and DFG for the Ph.D. grant support for A.V. Shirsath and the funding of the overall project.

Appendix: Estimation of diffusion coefficients of oxygen in the porous media

The diffusion coefficient of oxygen was calculated in the gas diffusion layer (in both microporous substrates, MPS, and MPL) and in the catalytic layer (CL), in addition to permeability values of the GDL percolated by the gas mixtures. For this purpose, the binary diffusion coefficient $D_{O2,j}$ was calculated using the well-known relationship [29]:

$$D_{O2,j} = \frac{a}{P}\left[\frac{T}{\sqrt{T_{c,O2}T_{c,j}}}\right]^{b}\left(\frac{T_{c,O2}}{T_{c,j}}\right)^{5/12}\left(\frac{P_{c,O2}}{P_{c,j}}\right)^{1/3}\sqrt{\frac{1}{M_{O2}}+\frac{1}{M_j}} \qquad \text{(A1)}$$

with a = 2.75×10^{-8} m^2 s^{-1}, b = 1.823 for non-polar gases, T the temperature in K, P the pressure in atm, M_j is the molecular weight for species j in g mol^{-1}, $T_{c,j}$ and $P_{c,j}$ are the critical temperature and pressure for species j (in atm). Critical temperatures are 154.4 K, 126.06 K and 5.04 K for O_2, N_2 and He respectively. Critical pressures are 49.7 atm, 33.62 atm and 2.26 atm respectively for these three gases. The effective diffusivity of oxygen diluted in the gas in a porous medium was estimated from the binary diffusion coefficient $D_{O2,j}$ considering the porosity of the medium, ε (after a Bruggeman's relationship) and its tortuosity τ_{PM}:

$$D_{O2,j,eff} = \frac{\epsilon_{PM}^{1.5} D_{O2,j}}{\tau_{PM}} \qquad \text{(A2)}$$

where ε_{PM} and τ_{PM} are respectively the porosity and the tortuosity of the porous medium considered. Porosity, tortuosity, and pore diameter d_p were respectively taken at 0.60, 2 and 10 nm for the CL; corresponding values for the GDL components are reported in Table 2. Moreover, the Knudsen diffusion coefficient D_{Kn} has been estimated in nitrogen and helium considering the pore size of the layer considered, d_p:

$$D_{Kn} = \frac{d_p}{3}\sqrt{\frac{8RT}{\pi M}} \qquad \text{(A3)}$$

where R is the perfect gas constant and M is in kg/mol. The equivalent diffusion of oxygen in the diluting gas, $D_{O2,eq}$, and in the porous medium considered was calculated using Bossanquet's equation [30]:

$$\frac{1}{D_{O2,eq}} = \frac{1}{D_{O2,eff}} + \frac{1}{D_{Kn}} \qquad \text{(A4)}$$

The equivalent diffusivity of O_2 in the two diluting and in the three porous media are reported Table 2. In the three porous media considered, O_2 equivalent diffusivities is approximately 4 times larger in helium than in nitrogen. Diffusion characteristic time τ in the porous medium was calculated after:

$$\tau_{diff} = \frac{\left(d_p \tau_{PM}\right)^2}{D_{O2,eq}} \qquad \text{(A5)}$$

Literature cited

[1] Springer T.E., Zawodzinski T.A., Characterization of polymer electrolyte fuel cells using AC impedance spectroscopy, J. Electrochem. Soc. 143 (1996) 587-589. doi: 10.1149/1.1836485

[2] Brug C.J., van den Eeden A.L.G., Sluyters Rehbach M., Sluyters J.H., The analysis of electrode impedances complicated by the presence of a constant phase element, J. Electroanal. Chem. 176 (1984) 275-295. doi: 10.1016/s0022-0728(84)80324-1

[3] Barsoukov E., Macdonald J.R. Eds, Impedance spectroscopy: theory, experiments and applications, New Jersey, J. Wiley & Sons (2005).

[4] Orazem M.E., Tribollet B., Electrochemical impedance spectroscopy, 2nd Edition, New Jersey, J. Wiley & Sons (2017).

[5] Keller S., Özel T., Scherzer A-C., Gerteisen D., Gross U., Bebling C., Manoli Y., Characteristic time constants derived from the low frequency arc of impedance spectra of fuel cell stacks, J. Electrochem. Energy Conv. Storage 15 (2018) 021002. doi:10.1115/1.4038632.

[6] Malevich D., Hallop E., Peppley B.A., Pharoah J.G., Karan K., Investigation of charge-transfer and mass-transfer electrochemical impedance spectroscopy, J. Electrochem. Soc. 156 2 (2009) B216-B224. doi: 10.1149/1.3033408

[7] Schneider I.A., Bayer M.H., Wokaun A., Scherer G.G., Impedance Response of the Proton Exchange Membrane in Polymer Electrolyte Fuel Cells, J. Electrochem. Soc. 155 (2008) B783-B792. doi: 10.1149/1.2929823

[8] Yuan H., Dai H, Wei X, Ming P., Internal polarization process revelation of electrochemical impedance spectroscopy of proton exchange membrane fuel cell by an impedance dimension model and distribution of relaxation times, Chem. Eng. J. 418 (2021) 129358. doi:10.1016/j.cej.2021.129358.

[9] Fouquet N., Doulet C., Nouillant C., Dauphin-Tanguy G., Ould-Bouamama B., Model based PEM fuel cell state-of-health monitoring via ac impedance measurements, J. Power Sources, 159 (2006) 905-913. doi:10.1016/j.jpowsour.2005.11.035.

[10] Roy S.K., Orazem M.E., Analysis of flooding as a stochastic process in polymer electrolyte membrane (PEM) fuel cells by impedance techniques, J. Power Sources, 184 (2008) 212-219. doi:10.1016/j.jpowsour.2008.06.014

[11] Deslouis C., Gil O., Tribollet B., Vlachos G., Robertson B., Oxygen as a tracer for measurements of steady and turbulent flows, J. Appl. Electrochem. 22 (1992) 835-842. doi: 10.1007/BF01023727

[12] Bourkane S., Gabrielli C., Keddam M., Investigation of gold oxidation in a sulphuric medium: electro-gravimetric transfer function technique, Electrochim. Acta 38, 14 (1993) 1827-1835. doi: 10.1016/0013-4686(93)80304-I

[13] Niroumand A.M., Mérida W., Eikerling M., Saif M. Pressure-voltage oscillations as a

diagnostic tool for PEFC cathodes. Electrochem. Commun. 12 (2010) 122–124. doi:10.1016/j.elecom.2009.11.003.

[14] Hartmann P., Grübl D., Sommer H., Janek J., Bessler W.G., Adelhelm P. Pressure dynamics in metal − oxygen (Metal − Air) batteries: a case study on sodium superoxide cells. J. Phys. Chem. C 2 (2014) 1461–1471. doi:10.1021/jp4099478.

[15] Grübl D., Janek J., Bessler W.G. Electrochemical pressure impedance spectroscopy (EPIS) as diagnostic method for electrochemical cells with gaseous reactants: a model-based analysis. J. Electrochem. Soc. 163 (2016) A599–A610. doi:10.1149/2.1041603jes.

[16] Engebretsen E., Mason T.J., Shearing P.R., Hinds G., Brett D.J.L. Electrochemical pressure impedance spectroscopy applied to the study of polymer electrolyte fuel cells. Electrochem. Commun. 75 (2017) 60–63. doi:10.1016/j.elecom.2016.12.014.

[17] Shirsath A.V., Raël S., Bonnet C., Lapicque F. Electrochemical pressure impedance spectroscopy applied to polymer electrolyte membrane fuel cells for investigation of transport phenomena. Electrochim. Acta. 363 (2020) 137157. https://doi.org/10.1016/j.electacta.2020.137157.

[18] Shirsath A.V., Raël S., Bonnet C., Schiffer L., Bessler W., Lapicque F. Electrochemical pressure impedance spectroscopy for investigation of mass transfer in polymer electrolyte membrane fuel cells. Curr. Opin. Electrochem. 20 (2020) 82–87. doi:10.1016/j.coelec.2020.04.017.

[19] Yang S.C., Cutlip M.B., Stonehart P. Simulation and optimization of porous gas-diffusion electrodes used in hydrogen/oxygen phosphoric acid fuel cells—I. Application of cathode model simulation and optimization to PAFC cathode development. Electrochim. Acta 35 (1990) 869–878. doi:10.1016/0013-4686(90)90083-C.

[20] Rho Y.W. Mass transport phenomena in proton exchange membrane fuel cells using O_2/He, O_2/Ar, and O_2/N_2 mixtures, J. Electrochem. Soc. 141 (1994) 2084-2089. doi:10.1149/1.2055065.

[21] Williams M. V., Kunz H.R., Fenton J.M. Influence of convection through gas-diffusion layers on limiting current in PEM FCs using a serpentine flow field. J. Electrochem. Soc. 151 (2004) A1617-A1627. doi:10.1149/1.1789791.

[22] Cruz-Manzo S., Greenwood P. Study of oxygen diffusion in the cathode catalyst layer and gas diffusion layer for polymer electrolyte fuel cells with EIS. J. Electroanal. Chem. 892 (2021) 115270. doi:10.1016/j.jelechem.2021.115270.

[23] Belhadj M., Aquino A., Heng J., Kmiotek S., Raël S., Bonnet C., Lapicque F., Current density distributions in polymer electrolyte fuel cells: a tool for characterisation of gas distribution in the cell and its state of health", Chemical Engineering Science 185 (2018) 18-25. doi:10.1016/j.ces.2018.03.055

[24] Gérardin K., Rael S., Bonnet C., Arora D., Lapicque F., Direct coupling of PEM fuel cells to supercapacitors for higher durability and better energy management", Fuel Cells 18 (3) (2018) 315-325. doi: 10.1002/fuce.201700041

[25] Mukherjee M., Bonnet C., Lapicque F. Estimation of through-plane and in-plane gas permeability across gas diffusion layers (GDLs): Comparison with equivalent permeability in bipolar plates and relation to fuel cell performance. Int. J. Hydrogen Energy 45 (2020) 13428–13440. https://doi.org/10.1016/j.ijhydene.2020.03.026.

[26] Owejan J.P., Trabold T.A., Mench M.M., Oxygen transport resistance correlated to liquid water saturation in the gas diffusion layer of PEM furl cell, Int. J. Heat Mass Transfer 71 (2014) 585-592. doi:10.1016/j.ijheatmasstransfer.2013.12.059.

[27] Benner J., Mortazavi M., Santamaria A.D. Numerical simulation of droplet emergence and growth from gas diffusion layers (GDLs) in proton exchange membrane (PEM) fuel cell flow channels, ASME Int. Mech. Eng. Congr. Expo. Proc. (2019) 6A-144113. doi:10.1115/imece2018-86579.

[28] Kulikovski A., A model for local impedance of the cathode cide of PEM fuel fell with segmented slectrodes, J. Electrochem. Soc. 159(7) (2012) F294-F300. doi: 10.1149/2.066207jes

[29] Bird R.B., Stewart W.E., Lightfoot E.N. Transport phenomena, Wiley and Sons, New York (1960).

[30] Pollard W.G., Present R.D, On gaseous self-diffusion in long capillary tubes, Phys. Rev. 73 (1948) 752-774.

[31] Pant L.M., Mitra S.K., Secanell M. Absolute permeability and Knudsen diffusivity measurements in PEMFC gas diffusion layers and micro porous layers. J. Power Sources. 206 (2012) 153–160. doi:10.1016/j.jpowsour.2012.01.099.

Porous medium		Thickness (µm)	Pore size (µm)	Porosity ε	Tortuosity τ_p (**)	Permeability (***) (m^2)
34 BA		270	30	0.83	2	$3.5\ 10^{-11}$
29 BC	Macroporous layer	190	30	0.83	2	$2.7\ 10^{-13}$
	Microporous layer	40	0.06 (*)	0.60		

Table 1: Properties of the Sigracet GDLs used. (*) value recommended in [31]; (**) Postulated values. (***) Through-plane permeability of the GDL for nitrogen at 20°C [25]).

Layer	Nitrogen	Helium	ε	L (µm)	$\tau_{diff\ N2}$ (ms)	$\tau_{diff\ He}$ (ms)
	O_2 equivalent diffusivity ($m^2\ s^{-1}$)					
MPS	$1.67\ 10^{-06}$	$6.85\ 10^{-06}$	0.83	190	211	87
MPL	$9.46\ 10^{-07}$	$3.69\ 10^{-06}$	0.60	40	17	6.8
CL	$6.42\ 10^{-07}$	$2.17\ 10^{-06}$	0.60	10	1.8	0.6

Table 2: Estimated values for the equivalent diffusivities of O_2 in the FC conditions of temperature and pressure in the different porous media and for the two diluting gases. The calculation procedure is reported in the Appendix.

.

Figure

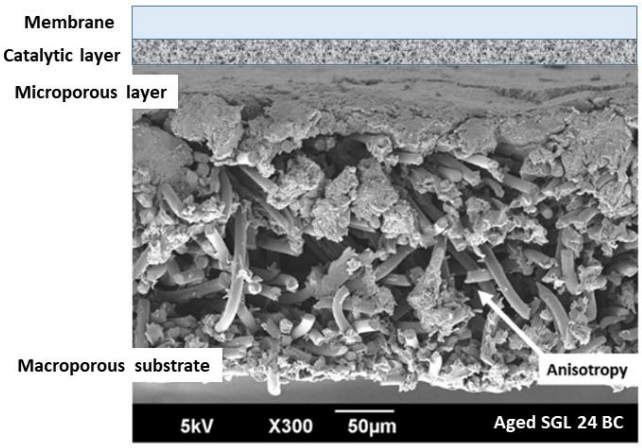

Figure 1

Figure 1: Schematic view of the layered structure of one FC compartment, with emphasis on MPL and MPS for the case of an aged GDL.

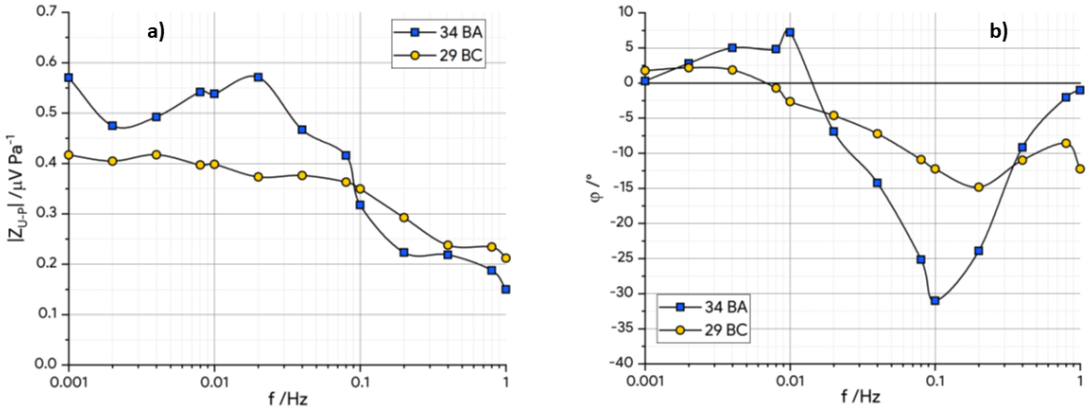

Figure 2

Figure 2: Modulus (a) and phase shift (b) of the voltage-pressure impedance of the fuel cell operated under pure oxygen (λ_{O2} = 11.9) at 0.2 A cm^{-2}, 55°C, with RH = 20 %.

Figure 3

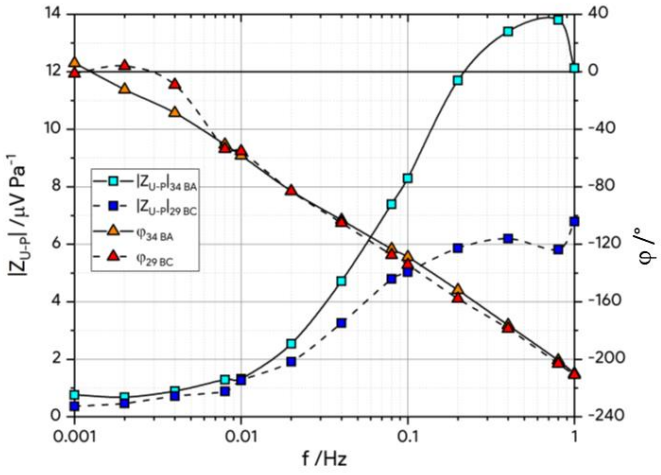

Figure 3: Modulus and phase shift of the voltage-pressure impedance of the fuel cell operated under air (λ_{O2} = 2.5) at 0.2 A cm^{-2}, 55°C, with RH = 20%. Comparison of the two GDLs inserted in the cathodic chamber.

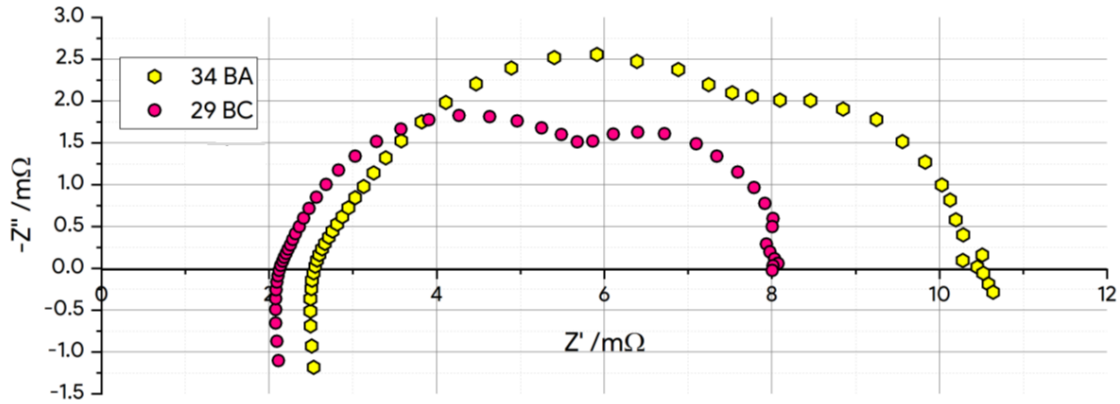

Figure 4

Figure 4: EIS spectra of the 100 cm^2 UBzM FC fed by air and operated at 0.2 A cm^{-2}, RH = 20%, λ_{O2} = 2.5. Comparison of the two GDLs inserted in the cathodic chamber.

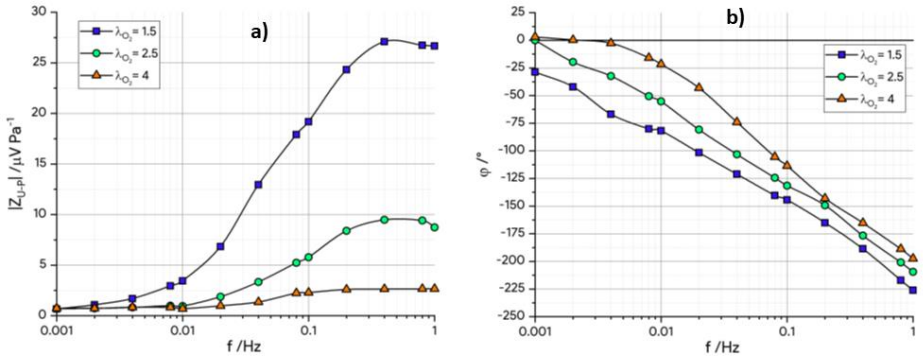

Figure 5

Figure 5: Modulus (a) and phase shift (b) of the voltage-pressure impedance of the fuel cell operated at 0.2 A cm^{-2}, 55°C, with RH = 20%, with various stoichiometric factors of air oxygen.

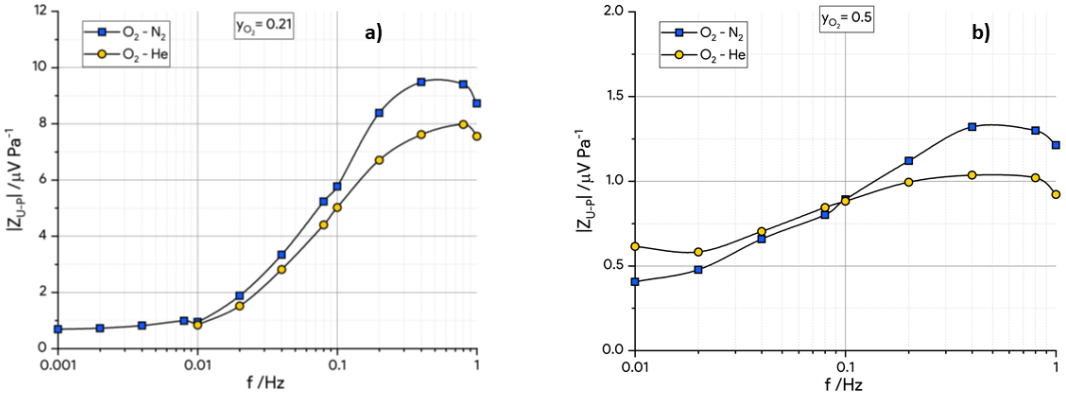

Figure 6

Figure 6: Modulus of the voltage-pressure impedance of the fuel cell operated at 0.2 A cm^{-2}, 55°C, with RH = 20%, by changing the O_2 content of gas mixture: y_{O2} = 0.21 in N_2 and in He (a), and y_{O2} = 0.50 in N_2 and in He (b).

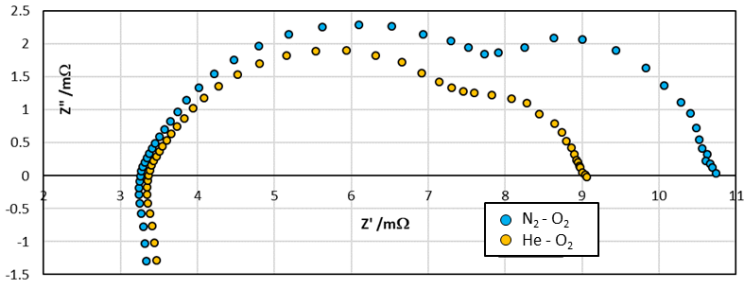

Figure 7

Figure 7: EIS spectra of the 100 cm^2 UBzM FC fed by air or heliox; 0.2 A cm^{-2}, RH = 20%, λ_{O2} = 2.5. y_{O2} = 0.21.